Fermi National Accelerator Laboratory

FERMILAB-Conf-97/008-E
DØ

Heavy Quark Results at DØ

David K. Fein
For the DØ Collaboration

Department of Physics, University of Arizona
Tucson, Arizona 85721

Fermi National Accelerator Laboratory
P.O. Box 500, Batavia, Illinois 60510

January 1997

Presented at the *2nd International Conference on Hyperons, Charm and Beauty Hadrons*, Montreal, Quebec, Canada, August 27-30, 1996

Operated by Universities Research Association Inc. under Contract No. DE-AC02-76CH03000 with the United States Department of Energy

Disclaimer

Distribution

Heavy Quark Results at DØ

FERMILAB-Conf-97/008-E

David K. Fein[a], for the DØ Collaboration

[a]Department of Physics, University of Arizona,
Tucson, AZ 85721, USA

Recent results on heavy quark physics from the DØ experiment at the Fermilab Tevatron Collider are reported. Topics included are top quark production and mass determination, bottom production and correlations, and charmonium production.

1. INTRODUCTION

The DØ detector, located at the Fermi National Accelerator Laboratory, is a large multipurpose detector designed to study a wide range of physics phenomena produced in proton-antiproton collisions at $\sqrt{s} = 1.8$ TeV. This paper summarizes recent heavy quark results from the DØ experiment. Results are presented on the top quark production cross section and top quark mass, inclusive beauty production and $b\bar{b}$ correlations, and finally charmonium production. A complete description of the DØ detector can be found in Ref. [1].

2. TOP PHYSICS

Since the announcement of the top quark discovery by DØ[2] and CDF[3] more than a year ago, DØ has nearly doubled its data sample to 100 pb^{-1} of integrated luminosity. In addition, methods for measuring top quark properties have improved. Both the top cross section and top mass analyses presented here assume that the top quark is pair-produced and decays 100% of the time into a W boson and a b-quark.

2.1. Top Cross Section

The top quark cross section measurement is based on seven different channels of $t\bar{t}$ decay. These include the dilepton channels where both W bosons decay leptonically ($e\mu$ + jets, ee + jets, $\mu\mu$ + jets) and the single lepton channels where just one W boson decays leptonically (e + jets and μ + jets). The single lepton channels are further subdivided according to whether or not an extra non-isolated muon is observed consistent with $b \to \mu + X$. The muon-tagged channels are denoted as e + jets/μ and μ + jets/μ.

Top events in the dilepton channels are selected by requiring two isolated leptons, two or more jets, and large missing transverse energy, $\not\!\!E_T$. In the single-lepton channels, one isolated lepton, large $\not\!\!E_T$, and three or more jets (with muon tag) or four or more jets (without tag) are required. A summary of the kinematic cuts for each channel is found in Table 1.

Each channel applies an H_T cut, where H_T is defined as the scalar sum of the jet E_T in the event. The definition of H_T for the dilepton channels is slightly modified to include the leading electron E_T. A series of special cuts are also employed to remove Z + jets backgrounds in the ee + jets, $\mu\mu$ + jets, and μ + jets/μ channels. A detailed description of these cuts can be found in Refs.[2,4]. In the single-lepton plus jets channels, cuts on aplanarity, $\mathcal{A}$, and E_T^W are used to help remove backgrounds, where E_T^W is defined as the scalar sum of the E_T of the lepton and $\not\!\!E_T$.

The acceptance for $t\bar{t}$ events was calculated using the ISAJET[5] Monte Carlo and a detector simulation using the GEANT[6] program. Systematic errors in the acceptance for $t\bar{t}$ events were determined using the HERWIG[7] event generator.

A total of 37 events in the seven channels survive all selection criteria with an expected background of 13.4±3.0 events, as shown in Table 2. The measured cross section as a function of top quark mass is shown in Fig. 1. Using the DØ measurement of the top quark mass (169 GeV/c^2),

Table 1
Kinematic requirements for top cross section event selection.

	High p_T Leptons		Jets		Missing E_T		Topological		
Channel	$E_T(e)$	$p_T(\mu)$	$N_{\rm jet}$	E_T(jet)	$\not\!\!E_T{}^{cal}$	$\not\!\!E_T$	H_T	$\mathcal{A}$	E_T^W
$e\mu$ + jets	15	15	2	20	20	10	120	-	-
ee + jets	20		2	20	25	-	120	-	-
$\mu\mu$ + jets		15	2	20	-	-	100	-	-
e + jets	20		4	15	25	-	180	0.065	$E_T^W > 60$ GeV
μ + jets		20	4	15	20	20	180	0.065	$E_T^W > 60$ GeV
e + jets/μ	20		3	20	20	-	110	0.04	-
μ + jetsμ		20	3	20	20	20	110	0.04	-

the top production cross section is 5.2±1.8 pb. As a cross check, the top production cross section was also calculated for the dilepton, tagged, and untagged single-lepton channels independently. All measurements were found to agree well within errors.

Table 2
Expected number of top events, $\langle N \rangle$, in the seven channels, based on the central theoretical $t\bar{t}$ production cross section of Ref.[8], for $M_t = 180$ GeV/c^2. Also shown are the expected background and number of observed events in each channel.

Channel	$\langle N \rangle$	Bkg	Data
$e\mu$ + jets	1.7±0.3	0.4±0.1	3
ee + jets	0.9±0.1	0.7±0.2	1
$\mu\mu$ + jets	0.5±0.1	0.5±0.3	1
e + jets	6.5±1.4	3.8±1.4	10
μ + jets	6.4±1.5	5.4±2.0	11
e + jets/μ	2.4±0.4	1.4±0.4	5
μ + jets/μ	2.8±0.9	1.1±0.2	6
Total	21.2±3.8	13.4±3.0	37

2.2. Top Mass

Results for the top quark mass measurement are shown here for the single-lepton + jets channel. The event selection for these channels is similar to those shown in Table 1, with the exception that each event is required to have at least four jets and no H_T or $\mathcal{A}$ cuts are applied. This results in a total of 8 events with a μ-tag and 85 without.

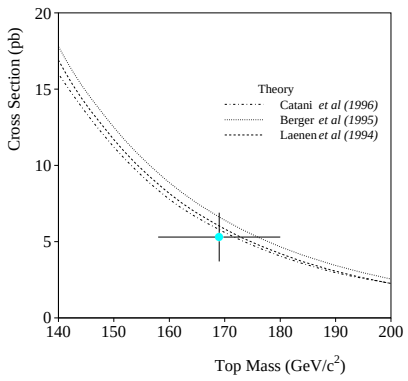

Figure 1. Preliminary $t\bar{t}$ production cross section as a function of top quark mass.

For each event, a mass (m_{fit}) is calculated assuming that the event is from a $t\bar{t}$ pair and that the four jets are either from $W \rightarrow q\bar{q}$ or the b jets. Of the 24 possible solutions (12 for tagged events) for m_{fit}, only events with a mass fit solution with $\chi^2 < 7$ are kept. This leaves 73 events in the sample. This sample is still highly contaminated with W + jets events. To distinguish $t\bar{t}$ events from the background, four kinematic variables have been identified that have very different distributions for signal and background[9]:

$v_1 \equiv \not\!\!E_T$

$$v_2 \equiv \mathcal{A} \equiv \frac{3}{2} \cdot \text{least eigenvalue of } \mathcal{P}$$

$$v_3 \equiv \frac{H_{T2} \equiv H_T - E_T^{j\,1}}{H_{\parallel}}$$

$$v_4 \equiv \frac{K_{T\min} \equiv (\text{min of } 6\ \Delta\mathcal{R}_{jj}) \cdot E_T^{\text{lesser } j}}{E_T^W},$$

where $\Delta\mathcal{R}_{jj}$ is the distance in η, ϕ between any two jets, $\mathcal{A}$ is the aplanarity, $\mathcal{P}$ is the normalized momentum tensor of the jets and the W in the laboratory frame, and $H_{\parallel}$ is the scalar sum of $|p_z|$ of the jets, charged lepton, and neutrino.

In order to maximize the differences between signal and background, we construct a top likelihood discriminant, $\mathcal{D}$, using the normalized signal to background ratios of $v_1 - v_4$. To determine the signal to background ratio and the most likely value of m_t, the data and Monte Carlo are binned in 10 GeV bins of m_{fit} and six regions of top quality:
1) All μ-tagged events,
2) $H_{T2} \geq 90$ GeV, $\mathcal{D} \geq 0.59$,
3) $H_{T2} \geq 90$ GeV, $0.43 \leq \mathcal{D} < 0.59$,
4) $H_{T2} \geq 90$ GeV, $0.27 \leq \mathcal{D} < 0.43$,
5) $H_{T2} \geq 90$ GeV, $\mathcal{D} < 0.27$,
6) $H_{T2} < 90$ GeV.
Figure 2 shows these distributions for a Monte Carlo background sample, a Monte Carlo $t\bar{t}$ sample, and the data. The entire sample of events, all six regions, is referred to as the PR (precut) sample, and contains an estimated signal-to-background ratio (S/B) of 1:2. As seen in Fig. 2, the first three regions are $t\bar{t}$ enriched and have S/B≈2:1. This subsample is referred to as the LB (low bias) sample.

To extract m_t, we maximize a Poisson-statistics likelihood function using discrete values of m_t. Using this likelihood function, the number of signal (n_s) and the number of background (n_b) events are found which maximized the likelihood for the PR sample as a function of m_t. Once n_s was determined for the PR sample, the same procedure was repeated for the LB sample but with n_s constrained within errors to the amount expected from the fit to the PR sample. The five points closest to the minimum of the likelihood function were fitted to a quadratic form to find the minimum value, and the closest nine points

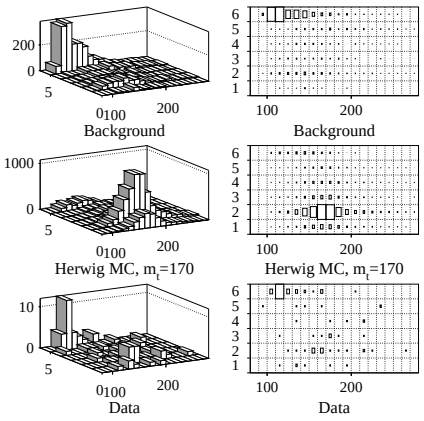

Figure 2. Scatter plot of background, $t\bar{t}$ Monte Carlo, and the data as a function of top quark mass and top quality bins (see text).

to a cubic to determine the uncertainty. The results of this fit are shown in Fig. 3, and give a top quark mass of 169±8(stat)±8(sys).

3. BOTTOM PHYSICS

The study of b-quark production in high energy $p\bar{p}$ collisions provides a benchmark test of perturbative QCD. The next-to-leading order (NLO) calculations of inclusive b and differential $b\bar{b}$ production cross sections have been available for some time[10,11]. Previous measurements of the inclusive b-quark production[12,13] cross section indicate disagreements in the overall normalization between data and the NLO calculations. Because of these uncertainties, it is important to have a firm understanding of the measured b-quark production cross section.

DØ detects b-quarks through their semileptonic decays into high p_T (transverse momentum with respect to the beam) muons. In addition, some DØ measurements make use of the fact that muons originating from b-quarks are accompanied by hadrons from fragmentation and decay of the parent b-quark (jets). The characteristics of the muons and accompanying jets can be used to further identify b-quarks.

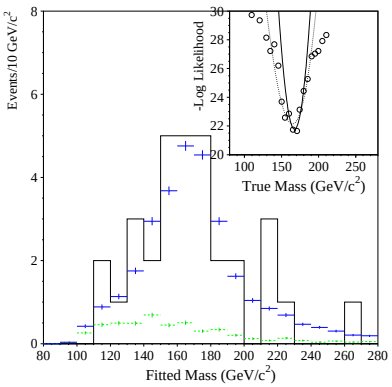

Figure 3. Distribution of m_{fit} for the LB data sample, where the solid(dashed) crosses are predictions from fitted values for the sum of signal and background(background only). Also shown is the likelihood as a function of m_t.

3.1. Inclusive b-Quark Production

The inclusive b-quark production cross section for $|y^b| < 1$ is measured using four different processes:

- Inclusive muon: $p\overline{p} \rightarrow b\overline{b}X \rightarrow \mu X$;
- Muon + jets: $p\overline{p} \rightarrow b\overline{b}X \rightarrow \mu +$ jets;
- Dimuon + jets: $p\overline{p} \rightarrow b\overline{b}X \rightarrow \mu\mu +$ jets;
- J/ψ production: $p\overline{p} \rightarrow J/\psi X \rightarrow \mu\mu X$.

The cross sections measured using the inclusive muon sample[14] and the J/ψ sample[15] have been published.

Figure 4 shows the results for the integrated b-quark production cross section as a function of p_T^{min} for $|y^b| < 1$. Also included is the NLO QCD prediction[10] using $m_b = 4.75$ GeV/c^2 and the MRSD0[16] structure functions with $\Lambda^5_{\overline{MS}} = 140$ MeV. The theoretical uncertainty results from varying the mass of the b-quark from $4.5 < m_b < 5.0$ GeV/c^2, the QCD mass scale between $100 < \Lambda^5_{\overline{MS}} < 187$ MeV, and the factorization and renormalization scale, μ, in the range $\mu_0/2 < \mu < 2\mu_0$, where $\mu_0^2 = m_b^2 + \langle p_T^b \rangle^2$. While all of the measurements agree with each other and with the shape of the QCD prediction, they systematically lie above the central QCD prediction, but still within experimental and theoretical uncertainties.

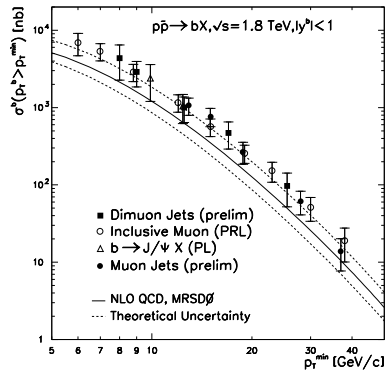

Figure 4. DØ inclusive b-quark measurements. Also shown is the NLO QCD calculation.

3.2. Forward $b \rightarrow \mu$ Production

A measurement of the $b \rightarrow \mu$ production cross section for forward muons is interesting because the b-quark production mechanisms may vary as a function of the b-quark rapidity. In addition, forward b production is sensitive to smaller values of Feynman x.

DØ has measured the forward $b \rightarrow \mu$ production cross section for muons in the forward rapidity range, $2.4 < |y^\mu| < 3.2$. By requiring each muon to have a large number of muon chamber hits, matching minimum ionizing energy in the calorimeter, and sufficient momentum kick from the magnetized iron toroid, combinatorial backgrounds contributing to the final data sample are estimated to be less than 2%. A total number of 3224 muon candidates survive.

The inclusive muon cross section was calculated

using

$$\frac{d\sigma^{\mu}}{dp_t^{\mu}dy} = \frac{1}{L\Delta y\Delta p_T}\frac{N^{\mu}f_p}{\epsilon}, \quad (1)$$

where f_p is a correction factor to account for momentum smearing. The π/K decay spectrum portion of the inclusive muon spectrum was obtained using ISAJET and subtracted. The ISAJET π/K spectrum is found to be in agreement with the charged particle spectrum measured by the CDF collaboration[17] in the central region, $|\eta| < 1$. In addition, the ISAJET π/K decay spectrum matches the data in the lowest p_T^{μ} bin (2-3 GeV/c), which should be dominated by these decays. The excess cross section above the π/K contribution is attributed to b- and c-quark decay.

The fraction of muons from b decays to those from both b and c decays was determined using ISAJET. The total b- and c-quark cross sections were separately normalized to NLO QCD calculations[11]. The differential muon cross section from b decays can then be found by multiplying this fraction by the π/K decay subtracted inclusive muon spectrum. This cross section is shown in Fig. 5 with the NLO QCD calculation using the MRSA'[16] structure functions. In the forward region, the data are roughly a factor of four above the central values of the theory.

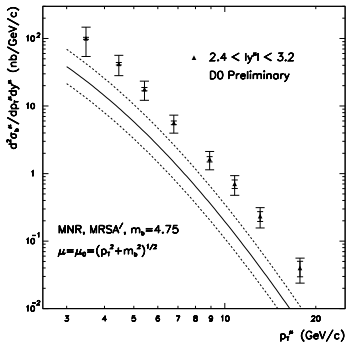

Figure 5. The forward $b \rightarrow \mu$ cross section for $2.4 < |y^{\mu}| < 3.2$.

3.3. $b\bar{b}$ Correlations

A measurement of the differential $b\bar{b}$ cross section gives further information on the underlying QCD production mechanisms by studying the topological correlation between the two b-quarks. The difference between the azimuthal angle between the b and the $\bar{b}$-quarks (or equivalently, between the decay muons), allows us to differentiate between the contributing QCD production mechanisms. These contributions include leading order diagrams (flavor creation) and next-to-leading order diagrams (flavor excitation and gluon splitting). There are also contributions from interference terms. Figure 6 shows the expected $\Delta\phi^{\mu\mu}$ distributions for the different production mechanisms after dimuon cuts using the ISAJET Monte Carlo. From Fig. 6 we see that contributions from higher order processes are expected in the region of $\Delta\phi^{\mu\mu} < 140^{\circ}$, where the leading order contribution is small.

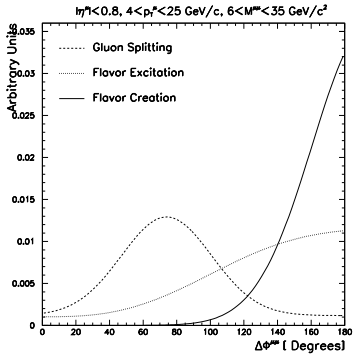

Figure 6. The ISAJET $\Delta\phi^{\mu\mu}$ distributions for the different production mechanisms.

In this analysis, dimuon events are selected where each muon has an associated jet. Additionally, the invariant mass of the dimuon pair must be between $6 < M^{\mu\mu} < 35$ GeV/c^2. The lower limit of this cut removes dimuons resulting from the cascade decay of a single b-quark and J/ψ decays, while the upper limit reduces dimuon de-

cays of the Z boson. Each muon must also satisfy the kinematic cuts $|\eta^\mu| < 0.8$ and $4 < p_T^\mu < 25$ GeV/c. A total of 397 events pass all selection criteria.

Backgrounds in this data sample include the semileptonic decay of $c\overline{c}$ pairs, events in which one or both of the muons are produced by in-flight decays of π or K mesons, and a small contribution from cosmic ray muons passing through the detector. Muons from Drell-Yan and Υ decays are not expected to have jets associated with them, so their contribution is negligible.

The $b\overline{b}$ signal is extracted using a maximum likelihood fit using four different input distributions. From this fit, we obtain the number $b\overline{b}$ events in each bin. The dimuon cross section originating from $b\overline{b}$ production is shown in Fig. 7. Also shown is the NLO QCD prediction that we have determined using the HVQJET[18] Monte Carlo. HVQJET is a direct implementation of the NLO QCD calculation which uses a modified version of ISAJET for hadronization, particle decays, and modeling of the underlying event. The prediction shown in Fig. 7 includes only the gluon-gluon initiated subprocesses but other subprocess contributions are expected to be small.

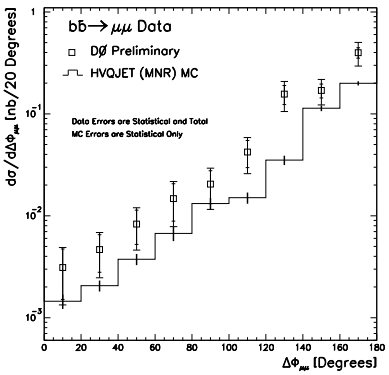

Figure 7. The $\Delta\phi^{\mu\mu}$ spectrum for $b\overline{b}$ production compared to the HVQJET prediction.

The data show a clear excess above the HVQJET prediction but agree with the overall shape. This is in agreement with the inclusive b-quark cross section results. Figure 7 also shows clear evidence for contributions from higher order processes.

4. CHARM PHYSICS

Charm physics at DØ has centered around the study of bound $c\overline{c}$ states. One picture[19] of charmonium production at the Tevatron is thought to include the following elements: B-hadron decays into J/ψ and χ_c, direct production (gluon fusion) into J/ψ and χ_c, and gluon and charm fragmentation into color singlet J/ψ and χ_c via color singlet and color octet $q\overline{q}$ pairs.

The B-hadron decays and gluon fusion components of bound $c\overline{c}$ production are well understood. The gluon and charm fragmentation components were added to explain why the measured J/ψ cross section at the Tevatron lay above the sum of the B-hadron decay and direct production components. Even after the gluon and charm fragmentation contributions are added in, the inclusive prompt ψ' data from CDF remained a factor of 30 above the theoretical predictions. Recent efforts by theorists to explain this discrepancy include charmonium production through fragmentation of the color octet components of its wave function[20]. The absolute normalization of the color octet contribution must be fixed by data however.

4.1. Central J/ψ and χ_c Production

J/ψ's in the central region, $|\eta^{J/\psi}| < 0.6$, were detected through their decay into dimuons. Trigger and muon quality cuts are similar to those imposed in the previous analysis. The invariant mass of the dimuon pair was required to be less than 6 GeV/c^2. For data collected during the 1992-1993 Tevatron collider run, 1146 dimuon events remain. The total number of J/ψ's in this sample was determined using a maximum likelihood fit. The theoretical J/ψ transverse momentum distribution, with the color octet term adjusted to fit the CDF prompt ψ' data, describes the measured J/ψ spectrum well.

The fraction of J/ψ's from B decays is determined by an impact parameter analysis using muons which have matching tracks in the central drift chamber and vertex detector. We find that the fraction of J/ψ's from B decays, f_b, is $f_b = 0.35 \pm 0.09(\text{stat}) \pm 0.10(\text{sys})$ for $\langle p_T^{J/\psi} \rangle = 11.8$ GeV/c. These results were used to extract the b-quark cross section shown in Sec. 3.1.

To determine the fraction of J/ψ's from χ_c a search is made for photons with $E_\gamma > 1$ GeV in a cone of $\Delta R = 2.0$ about the dimuon direction. The χ_c signal is measured by fully reconstructing the decay chain, $\chi_c \rightarrow J/\psi\ \gamma; J/\psi \rightarrow \mu\mu$. The distribution $\Delta M = M^{\mu\mu\gamma} - M^{\mu\mu}$ is fit to a Gaussian plus a background shape determined from the data. This fit is shown in Fig. 8. A total of 74 ± 13 χ_c events are found from the fit.

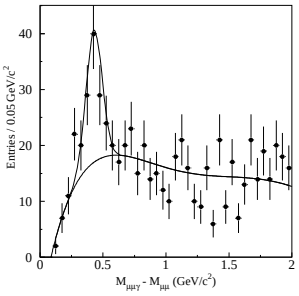

Figure 8. The $\Delta M = M^{\mu\mu\gamma} - M^{\mu\mu}$ distribution for candidate $\chi_c \rightarrow J/\psi\ \gamma$ events.

Using this fit, and correcting for photon efficiency and acceptance, we find the fraction of J/ψ's from χ_c decays to be $f_\chi = 0.32 \pm 0.07(\text{stat}) \pm 0.07(\text{sys})$. Correcting for the fraction of χ_c coming from B decays (0.08 ± 0.03) we determine a fraction $f = (1 - f_b - f_\chi + f_{B \rightarrow \chi}) = 0.41 \pm 0.17$ of all J/ψ's that do not originate from either B of χ_c decays for $\langle p_T^{J/\psi} \rangle = 11.8$ GeV/c. Therefore, prompt J/ψ production is not dominated by χ_c decay as expected from gluon fragmentation models. This is consistent with the color octet model.

4.2. Forward J/ψ Production

The forward J/ψ production cross section was measured using data collected during the 1994-1995 Tevatron run. Measuring the η dependence of J/ψ production is interesting because the relative contributions of J/ψ production mechanisms may vary with J/ψ rapidity. In addition, the forward J/ψ's $(2.5 < |\eta^{J/\psi}| < 3.7)$ probe smaller Feynman x values of the gluon structure function than those J/ψ's produced in the central region $(|\eta^{J/\psi}| < 0.6)$.

The offline selection criteria for forward J/ψ's is identical to those described above for the forward $b \rightarrow \mu$ cross section. A total of 1234 events remain after all cuts. This sample is then divided into six different $\eta^{J/\psi}$ regions, with a clear J/ψ signal seen in each region. The number of J/ψ's in each $p_T^{J/\psi}$ bin is determined by fitting the dimuon invariant mass to the sum of a Gaussian function plus physics motivated background in the mass range $2 < M^{\mu\mu} < 6$ GeV/c^2. After acceptance, efficiency, and muon momentum corrections, we obtain the differential cross section for forward J/ψ production. The results for $Br \cdot d\sigma/dp_T^{J/\psi}/\Delta\eta$ are shown in Fig. 9. This is the first measurement at a hadron collider of the inclusive J/ψ cross section at large $\eta^{J/\psi}$. The solid curve in Fig. 9 is the predicted contribution from B decays only.

Combining the results for both central and forward J/ψ data, the differential cross section, $Br \cdot d\sigma/d\eta^{J/\psi}$, for $p_T^{J/\psi} > 8$ GeV/c, is given in Fig. 10. The production cross section in the forward region, $\eta^{J/\psi} \approx 2.9$, is smaller than that in the central region by about a factor of 5. Also shown in Fig. 10 is the B decay contribution to J/ψ production, which shows a similar dependence in $\eta^{J/\psi}$.

5. CONCLUSIONS

We have reported on a number of recent measurements by the DØ collaboration on heavy flavor physics. The top production cross section, 5.2 ± 1.8 pb, is found to be in good agreement

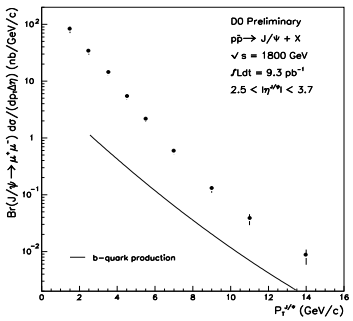

Figure 9. The forward J/ψ production cross section for $2.5 < |\eta^{J/\psi}| < 3.7$.

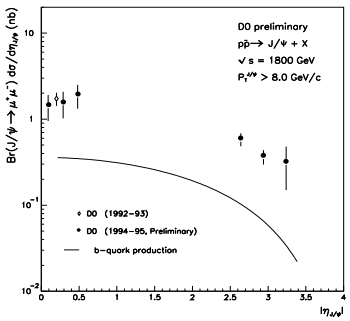

Figure 10. The J/ψ production cross section as a function of $\eta^{J/\psi}$.

with theoretical predictions. In addition, the top mass of 169 ± 8(stat)±8(sys) is calculated using the single-lepton + jets channel. The inclusive b-quark production cross section has been measured using four different channels. In all channels, the measured cross section is a factor of two larger than the NLO QCD calculation in the central rapidity region, while an even larger discrepancy is found in the forward region. For charmonium production, prompt J/ψ production appears not to be dominated by χ_c decay.

REFERENCES

1. DØ Collaboration, S. Abachi *et al.*, *Nucl. Instr. Meth.* **A338**, 185 (1994).
2. DØ Collaboration, S. Abachi *et al.*, *Phys. Rev. Lett.* **74**, 2632 (1995).
3. CDF Collaboration, F. Abe *et al.*, *Phys. Rev. Lett.* **74**, 2626 (1995).
4. DØ Collaboration, S. Abachi *et al.*, *Phys. Rev.* D **52**, 4877 (1995).
5. F. Paige and S. Protopopescu, BNL Report No. BNL38034, 1986 (unpublished), v.7.1.
6. F. Carminati *et al.*, *GEANT Users Guide*, CERN Program Library, December 1991 (unpublished).
7. G. Marchesini *et al.*, *Comput. Phys. Commun.*, **67**, 465 (1992).
8. E. Laenen, J. Smith, and W. van Neerven, *Phys. Lett.* B **321**, 254 (1994).
9. S. Protopopescu, *Measurement of the Top Quark Mass at DØ*, submitted to Proceedings of the 28th International Conference on High Energy Physics, Warsaw (1996).
10. P. Nason, S. Dawson, and R.K. Ellis, *Nucl. Phys.* **B303**, 607 (1988); **B327**, 49 (1989).
11. M. Mangano, P. Nason, G. Ridolfi, *Nucl. Phys.* **B373**, 295 (1992).
12. UA1 Collaboration, C. Albajar *et al.*, *Phys. Lett.* B **256**, 121 (1991); *Z. Phys.* C **61**, 41 (1994).
13. CDF Collaboration, F. Abe *et al.*, *Phys. Rev. Lett.* **68**, 2403 (1992); **69**, 3704 (1992); **71**, 500 (1993); **71**, 2396 (1993); **71**, 2537 (1993).
14. DØ Collaboration, S. Abachi *et al.*, *Phys. Rev. Lett.* **74**, 3548 (1995).
15. DØ Collaboration, S. Abachi *et al.*, *Phys. Lett.* **B370**, 239 (1996).
16. A. Martin, R. Roberts, and J.W. Sterling, *Phys. Rev.* D **47**, 867 (1993).
17. CDF Collaboration, F. Abe *et al.*, *Phys. Rev. Lett.* **61**, 1819 (1988).
18. M.M. Baarmand, DØ Note 2517, 1995.
19. M. Mangano, Proceedings of the 10th Topical Workshop on $p\overline{p}$ Collisions (AIP Conference Proceedings 357), 120 (1995).
20. E. Braaten and S. Fleming, *Phys. Rev. Lett.* **74**, 3327 (1995).